Modeling and Stability Analysis of Back-to-Back Converters in Networked Microgrids

1st Mobin Naderi, 2nd Yousef Khayat, 4th Qobad Shafiee, 6th Hassan Bevrani

Department of Electrical Engineering
Smart/Micro Grids Research Center, University of Kurdistan
Sanandaj, Iran
m.naderi@eng.uok.ac.ir, y.khayat@eng.uok.ac.ir, q.shafiee@uok.ac.ir, bevrani@uok.ac.ir

3rd Rasool Heydari, 5th Tomislav Dragicevic, 7th Frede Blaabjerg

Department of Energy Technology
Aalborg University
Aalborg, Denmark
rah@et.aau.dk, tdr@et.aau.dk, fbl@et.aau.dk

***Abstract*—This paper provides a small-signal model and stability analysis of interconnected AC microgrids (MGs) connected through back-to-back converters (BTBCs). The proposed modeling method of the networked microgrids (NMGs) is derived and it is generalized for any number of NMGs through BTBCs. Different BTBC control parts are analyzed to study their impact on the NMG stability. The eigenvalue analysis and participation matrix are employed to identify dynamic modes of BTBC DC voltage controller. For two NMGs, main participating state variables and corresponding parameters in the dominant low-frequency modes (LFMs) are recognized, then acceptable ranges of the parameters are calculated using the sensitivity analysis (SA). The contribution of the control BTBC parameters including PLL and DC voltage controller parameters in the small-signal stability margin are shown. In addition, to show the BTBC control impact on the NMGs stability in the time domain, simulation results are provided for the two NMGs in SimPowerSystems/Matlab environment.**

***Index Terms*—Networked AC microgrids, back-to-back converters, small-signal modeling, Small-signal stability analysis, sensitivity analysis.**

I. Introduction

INDIVIDUAL MGs are new blocks of modern power grids, which integrate distributed energy resources (DERs) and localize the production and consumption of electricity. Each MG consists of a group of DERs, storage systems, loads, as well as protection and control devices that can be operated in both grid-connected and autonomous modes. MGs improve the stability, reliability, economic optimality and resiliency in comparison with individual DERs and provide auxiliary services for conventional distribution systems [1]–[3]. Although, the need for improving security, reliability, sustainability, flexibility and DER penetration level of individual MGs leads to the solution of networking [3], [4]. If NMGs are operated stably and optimally, they can propose many advantages to local consumers and distribution systems.

NMGs can be constructed in various structures. AC/DC MGs, AC/DC interlinking lines (ILs), interlinking devices, type of networking, and control and communication methods leads to different NMG structures [5]. Fully DC NMGs networked by DC ILs [6], [7], fully AC NMGs networked through AC ILs [8]–[11], and mixed DC and AC NMGs networked through DC/AC ILs and DC-AC converters [12], [13] or more complicated power-electronics devices [14] are presented in the literature.

In order to interconnect AC MGs, BTBCs, circuit breakers and static switches can be used as interlinking devices. circuit breakers and instantaneous static switches are used further in the literature that can only network AC MGs with same voltages and frequencies [8], [10], [15]–[17]. In such NMGs a synchronizing algorithm is required to interconnect MGs, and power exchange can be controlled by changing droop coefficients of primary controllers [8]. More flexible power exchange can be achieved by networking AC MGs using BTBCs [9], [11], [18], [19]. Moreover, independently control of frequency and voltage of each MG [20], [21], power quality improvement by reactive/harmonic power interchange control [22], and integration of multiple AC MGs with different nominal voltages/frequencies [18], [19], [21] can be addressed for NMGs via BTBCs. In addition, several applications of BTBCs for bidirectional power flow between MGs and the utility grid are reported [23], [24].

Small-signal modeling (SSM) is a well-known method to identify the small-signal behaviour of systems. SSM is employed for MGs performance and stability analysis as well as controller design [25]–[28]. It has developed for NMGs recently [10], [15], [16], [29], [30]. The small-signal stability

978-1-7281-4878-6/19/$31.00 ©2019 IEEE

of NMGs with circuit breakers or static switches has been analyzed in the literature [17]. Another stability analysis is performed to study the impact of different interconnecting points within a distribution network on NMG formation [10]. A parametric criterion for NMG stability is achieved by applying Lyapunov stability on the simplified droop-based NMG model [31]. In contrast, a detailed SSM of PV-based NMGs is proposed considering the dynamics of the PV controllers and DER DC sides [16]. In [15], authors have presented a two-layer, four-level distributed control strategy for NMGs, then they have analyzed the impact of the proposed controller on the stability. Similar work have been presented for a distributed voltage control and power management of NMGs [30]. Only stability assessment of NMGs with BTBCs refers to multiple MGs connecting to the ideal main grid, where main challenges of NMGs such as power sharing and voltage/frequency control do not reveal [23].

This paper develops the small-signal modeling and stability for BTBC-interconnected AC MGs, where BTBCs play a significant role in NMG control and stability. Distinctive features of this paper can be listed as: 1) in comparison with presented methods in [15], and [16], a detailed SSM method is proposed for NMGs, which can simply be generalized for any number of MGs and interlinks by applying *sysic* function of Robust Control Toolbox (RCT) in MATLAB. 2)The stability is assessed using EVA and PM for two NMGs typically in order to determine the frequency ranges of BTBC state variables. 3)In the proposed modeling and provided stability analysis of the NMGs, BTBCs are included as interlinking devices, which are not taken into account in the literature. 4) Most effective state variables and corresponding parameters in the LFMs are recognized, then acceptable ranges of the BTBC parameters are calculated using SA to operate the NMGs robustly stable.

II. Small-Signal Modeling of NMGs

Fig. 1 shows a general configuration of NMGs, where are connected through BTBCs. To assess their stability, a comprehensive model is needed.

The proposed modeling method for NMGs consists of two main steps: 1) main modules comprising autonomous AC MGs, AC ILs and interface BTBCs should be modeled in using a state space representation separately, and 2) All interconnections among modeled modules should be considered using *sysic* function of RCT/MATLAB. The first step is realized through Sections II.A, II.B and II.C. The second step is accomplished in Section II.D.

A. Modeling of Autonomous MGs

Fig. 2 shows a typical autonomous AC MG in a general form, which *m* DERs supply a common load located integrally at the PCC through RLC filters and coupling lines. Each DER is controlled by a three-stage cascade control including power, voltage and current control loops. Algorithms where cascaded organization of control loops are avoided to speed the dynamic response [32]. All DER controls are coordinated by droop characteristics. DERs are considered as VSCs, which can be

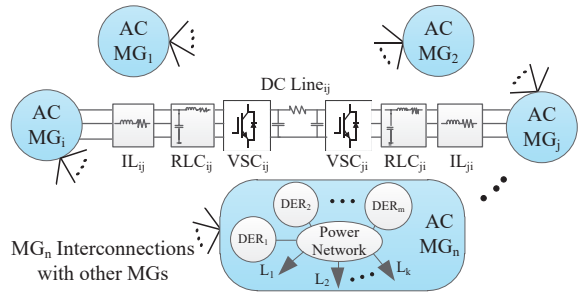

Fig. 1. AC Networked MGs using back-to-back converters, DC and AC interlinking lines.

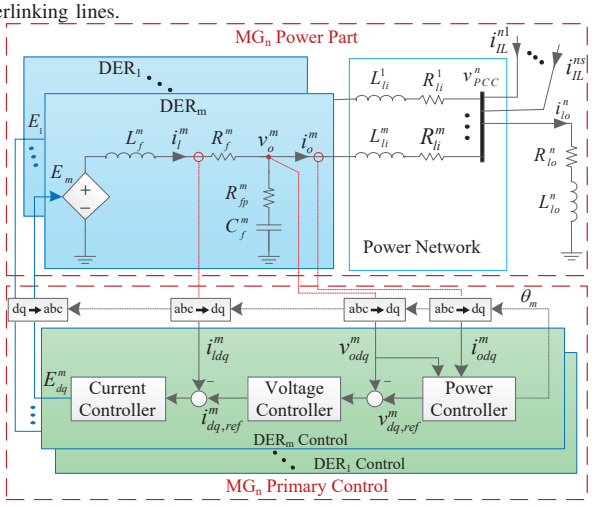

Fig. 2. A typical autonomous AC MG including Power components: DERs, power network and Load, and Primary control level: power, voltage and current controllers.

modelled as dependent voltage sources using ideal averaging model. The detailed model of an autonomous AC MG shown in Fig. 2, is obtained by modeling all power and control parts as following sub-sections.

1) DER Power Part: Dynamics of output RLC filter of VSC can be given as follows:

$$\begin{aligned} \dot{X}^m_{DP} &= A^m_{DP}X^m_{DP} + B^m_{DP}U^m_{DP} + B^m_{PN}U^m_{PN}, \\ Y^m_{DP} &= C^m_{DP}X^m_{DP} + D^m_{DP}U^m_{DP} + D^m_{PN}U^m_{PN}, \end{aligned} \tag{1}$$

where $X^m_{DP} = [\Delta i^m_{ldq} \ \Delta v^m_{odq}]^T$, the control input $U^m_{Dr} = [\Delta E^m_{dq} \ \Delta\omega_m]^T$, the disturbance input $U^m_{DP} = i^m_{odq}$, and the matrices can be found in [33].

2) Power Network: The dynamic model of the m'th line connected to the PCC, as shown in Fig. 2, is expressed as:

$$\begin{aligned} \Delta\dot{i}^m_{od} &= -\frac{R^m_{li}}{L^m_{li}}\Delta i^m_{od} + \omega_{m0}\Delta i^m_{oq} + \frac{1}{L^m_{li}}\Delta v^m_{od} \\ &\quad - \frac{1}{L^m_{li}}\Delta v^m_{pcc,d} + i^m_{oq0}\Delta\omega^n_{com}, \\ \Delta\dot{i}^m_{oq} &= -\omega_{m0}\Delta i^m_{od} - \frac{R^m_{li}}{L^m_{li}}\Delta i^m_{oq} + \frac{1}{L^m_{li}}\Delta v^m_{oq} \\ &\quad - \frac{1}{L^m_{li}}\Delta v^m_{pcc,q} - i^m_{od0}\Delta\omega^n_{com}, \end{aligned} \tag{2}$$

where $\Delta\omega^n_{com}$ is the perturbed frequency form of the MG$_n$'s common reference frame (CRF).

3) MG Load: Expression of the dynamics of the RL load of MG$_n$ in dq frame can be found by applying KVL, and then the state space is as follows:

$$\dot{X}^n_{ML} = A^n_{ML}X^n_{ML} + B^n_{ML}U^n_{ML},$$
$$Y^n_{ML} = C^n_{ML}X^n_{ML} + D^n_{ML}U^n_{ML}, \quad (3)$$

where $Y^n_{ML} = X^n_{ML} = \Delta i^n_{lo,dq}$, and $U^n_{ML} = v^n_{PCC,dq}$.

4) Power Controller: The power controller for each DER consists of a power calculator, low-pass filters (LPFs), $\omega - P$ and $V_d - Q$ droop mechanisms. Furthermore, the angle difference between the DER$_m$ reference frame with the CRF (δ_m) is considered as another state variable as follows:

$$\delta_m = \theta_m - \theta^n_{com} = \int (\omega_m - \omega^n_{com})dt, \quad (4)$$

where θ_m and ω_m are the voltage phase and frequency of the DER$_m$ and θ^n_{com} is the voltage phase of the DER$_1$, which the MG$_n$'s CRF is based on it. Hence, a state space representation is given as follows:

$$\dot{X}^m_{PC} = A^m_{PC}X^m_{PC} + B^m_{PDP}U^m_{PDP} + B^m_{PC}\Delta\omega^n_{com},$$
$$Y^m_{PC} = C^m_{PC}X^m_{PC}, \quad (5)$$

where $X^m_{PC} = [\Delta\delta_m \ \Delta P_m \ \Delta Q_m]^T, U^m_{PDP} = Y^m_{DP}, and Y^m_{PC} = [\Delta\omega_m \ \Delta v^m_{dq,ref} \ \Delta\delta_m]^T$. All matrices can be found in [33].

5) Voltage Controller: By considering a PI controller, a state space model for voltage controller can be given as [33]:

$$\dot{X}^m_{VC} = A^m_{VC}X^m_{VC} + B^m_{VC}U^m_{VC},$$
$$Y^m_{VC} = C^m_{VC}X^m_{VC} + D^m_{VC}U^m_{VC}. \quad (6)$$

6) Current Controller: Similar to the voltage controller, a state space description for the current controller can be expressed as follows, which the details can be found in [33].

$$\dot{X}^m_{CC} = A^m_{CC}X^m_{CC} + B^m_{CC}U^m_{CC},$$
$$Y^m_{CC} = C^m_{CC}X^m_{CC} + D^m_{CC}U^m_{CC}. \quad (7)$$

7) Common Reference Frame: Frequency interaction of DERs should be considered by a CRF [10], [25], [34]. Therefore, i^m_{odq} should be transformed to the CRF and the inverse transformation is needed for $v^n_{pcc,dq}$. Both the transformation and its inverse for linearized variables are as follows:

$$\Delta v_{DQ} = T_s.\Delta v_{dq} + T_{\delta 1}.\Delta\delta, \quad (8a)$$
$$\Delta v_{dq} = T_s^{-1}.\Delta v_{DQ} + T_{\delta 2}.\Delta\delta, \quad (8b)$$

where $\Delta\delta$ is the angle difference between the i'th reference frame and the CRF.

8) MG Interconnection and Complete Model: An intensive MG model can be given using *sysic* function, which can interconnect any number of DERs, coupling lines and loads. The state space representation is obtained as follows:

$$\dot{X}^n_{MG} = A^n_{MG}X^n_{MG} + B^n_{MG}U^n_{MG},$$
$$Y^n_{MG} = C^n_{MG}X^n_{MG} + D^n_{MG}U^n_{MG}, \quad (9)$$

where X^n_{MG} can be organized in any order such as

$$X^n_{MG} = [X^1_{DER} \ X^2_{DER} \cdots \overbrace{X^m_{PD} \ X^m_{PC} \ X^m_{VC} \ X^m_{CC}}^{X^m_{DER}}$$
$$X^1_{PL} \ X^2_{PL} \cdots X^m_{PL} \ X^n_{ML}]^T,$$

and it consists of $13m+2$ state variables for the MG structure shown in Fig. 2, where m is the number of DERs/lines. The current of all ILs to MG$_n$ are as the input i.e. $U^n_{MG} = [i^{n1}_{IL,dq} \cdots i^{ns}_{IL,dq}]^T$ and the MG$_n$ impact on the overall model of NMGs can be considered as $Y^n_{MG} = [\Delta\omega^n_{com} \ \Delta v^n_{pcc,dq}]$. The matrices can be calculated using module models, considering their interconnections and employing *sysic* function.

B. Interconnecting Line

The dynamics of interlinking lines are completely similar to the dynamics of the internal MG RL lines (2).

C. Back-to-Back Converter Modeling

In order to control power flow among AC MGs, BTBCs are used. Fig. 3(a) shows the block diagram of the BTBC control. The detailed model can be found by modeling all parts including LCL filters, common DC link, power and DC voltage controllers as well as PLLs. Then, the interconnections should be considered using *sysic* function.

1) AC Side: Fig. 3(b) shows the circuit model of the BTBC power part. Each AC side of the BTBC comprises an LCL filter, which its dynamics are presented in (1).

2) DC Side: The currents drawn from AC sides in order to form the dependent voltage sources, i.e. E^i_C and E^i_C, are modeled by current sources shown in Fig. 3(b). In addition, the DC line is modeled by a resistor in the BTBC DC side. By considering the capacitor voltages as state vector $X^{ij}_{Bdc} = [\Delta v^i_{dc} \ \Delta v^j_{dc}]^T$, and control inputs $U^{ij}_{Bdc} = [\Delta I^i_C \ \Delta I^j_C]^T$, A normal linear state space representation can be obtained with following matrices:

$$A^{ij}_{Bdc} = \begin{bmatrix} -\frac{1}{R^{eq}_{dc}C^i_{dc}} & \frac{1}{R^{eq}_{dc}C^i_{dc}} \\ \frac{1}{R^{eq}_{dc}C^j_{dc}} & -\frac{1}{R^{eq}_{dc}C^j_{dc}} \end{bmatrix},$$
$$B^{ij}_{Bdc} = \begin{bmatrix} \frac{R^i_{dc}}{R^{eq}_{dc}} - 1 & -\frac{R^j_{dc}}{R^{eq}_{dc}} \\ -\frac{R^i_{dc}}{R^{eq}_{dc}} & \frac{R^j_{dc}}{R^{eq}_{dc}} - 1 \end{bmatrix},$$

where $R^{eq}_{dc} = R^i_{dc} + R^j_{dc} + R^{ij}_{Ldc}$, and $C^{ij}_{Bdc} = I_2$.

3) Dependent Current and Voltage Sources: These sources are as transformations from AC/DC side to DC/AC side as follows:

$$I^i_C = P^i_C/v^i_{dc}, \quad (10)$$
$$E^i_C = (1/2)m_i v^i_{dc}, \quad (11)$$

where P^i_C is the produced AC power of VSC$_i$ and m_i is the PWM control signal shown in Fig. 3(a). By linearizing (10) and (11) the transformations can be calculated as follows:

$$\Delta I^i_C = T^i_{ac/dc}\begin{bmatrix} \Delta v^i_{dc} & \Delta E^i_{Cdq} & \Delta i^i_{fc,dq} \end{bmatrix}^T,$$
$$\Delta E^i_{Cdq} = T^i_{dc/ac}\begin{bmatrix} \Delta v^i_{dc} & \Delta m^i_{dq} \end{bmatrix}^T, \quad (12)$$

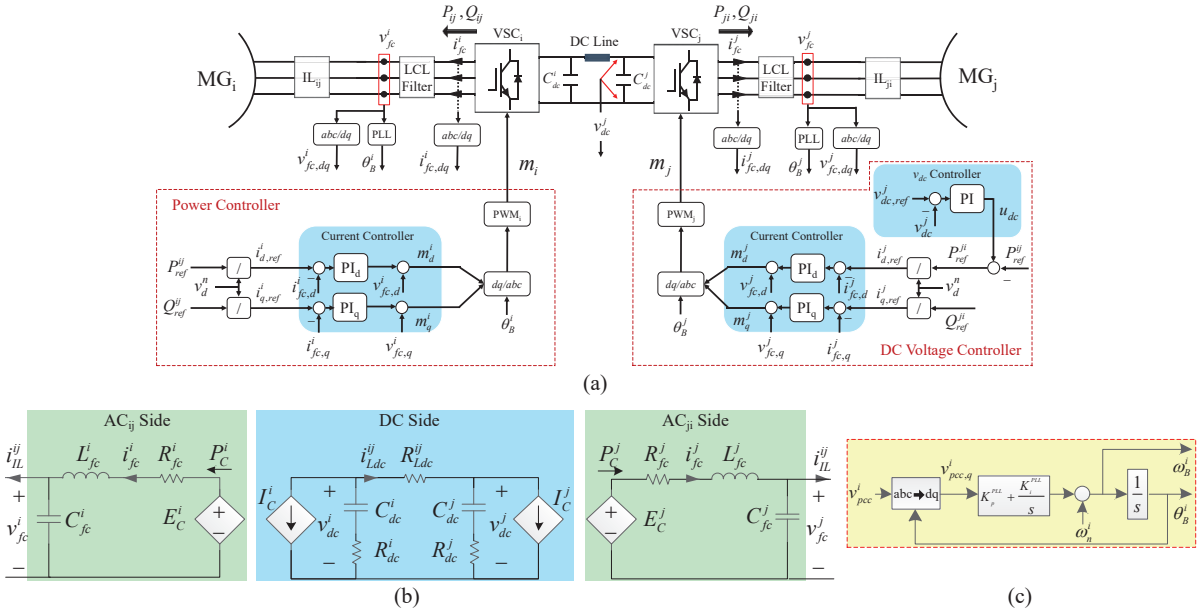

Fig. 3. Interlinking back-to-back converter: (a) control and operation block diagram, and (b) power part averaging model.

where

$$T^i_{ac/dc} = \frac{3}{2v^i_{dc0}}[-\frac{2}{3}I^i_{C0} \quad E^i_{Cd0} \quad E^i_{Cq0} \quad i^i_{fc,d0} \quad i^i_{fc,q0}], \quad (13)$$

$$T^i_{dc/ac} = \frac{1}{2}\begin{bmatrix} m^i_{d0} & v^i_{dc0} & 0 \\ m^i_{q0} & 0 & v^i_{dc0} \end{bmatrix}. \quad (14)$$

4) Power Controller: Similar to the PI current controller model of DERs, i.e. (7), a state space model for the power controller of the BTBC can be expressed.

5) DC Voltage Controller: In addition to the current controller, which can be modeled similar to (7), the V^j_{dc} controller is modeled with one state variable as follows:

$$\dot{X}^j_{DVC} = B^j_{DVC}U^j_{DVC},$$
$$Y^j_{DVC} = C^j_{DVC}X^j_{DVC} + D^j_{DVC}U^j_{DVC}, \quad (15)$$

where X^j_{DVC} is the integrator output, $U^j_{DVC} = \Delta v^j_{dc}, Y^j_{DVC} = \Delta i^{ref,j}_{fc,d}, B^j_{DVC} = K^{DVC}_i, C^j_{DVC} = [2/3v^i_{fc,d} \quad 0]^T$ and $D^j_{DVC} = [2K^{DVC}_p/3v^i_{fc,d} \quad 0]^T$.

6) Phase-Locked Loop: Two PLLs are needed to synchronize AC sides with the MGs through ILs. Fig. 3(c) displays the PLL structure. PI integrator output is considered as state variable. Another state variable is as $\delta^i_B = \theta^i_B - \theta^i_{com}$ to state all BTBC AC side dynamics into the corresponding CRF, e.g. VSC$_i$ dynamics into MG$_i$ CRF. Hence, the state space representation is as follows:

$$\dot{X}^i_{pll} = A^i_{pll}X^i_{pll} + B^i_{pll}U^i_{pll},$$
$$Y^i_{pll} = C^i_{pll}X^i_{pll}, \quad (16)$$

where $U^i_{pll} = [\Delta v^i_{pcc,q} \quad \Delta\omega^i_{com}]^T, Y^i_{pll} = [\Delta\omega^i_B \quad \Delta\delta^i_B]^T$ and

$$A^i_{pll} = \begin{bmatrix} 0 & 0 \\ 1 & 0 \end{bmatrix}, B^i_{pll} = \begin{bmatrix} K^{pll}_i & 0 \\ K^{pll}_p & -1 \end{bmatrix}, C^i_{pll} = \begin{bmatrix} 1 \\ 0 \end{bmatrix}^T,$$
$$D^i_{pll} = \begin{bmatrix} K^{pll}_p & 0 \end{bmatrix}.$$

7) Complete Interconnection of BTBC Modules: The overall state space of BTBC$_{ij}$ model is given as follows:

$$\dot{X}^{ij}_B = A^{ij}_B X^{ij}_B + B^{ij}_B U^{ij}_B,$$
$$Y^{ij}_B = C^{ij}_B X^{ij}_B + D^{ij}_B U^{ij}_B, \quad (17)$$

where X^{ij}_B is a 21×1 vector, including all BTBC state variables as

$$X^{ij}_B = [X^{ij}_{BP} \; X^i_{Bpc} \; X^j_{Bcc} \; X^j_{DVC} \; X^i_{PLL} \; X^j_{PLL}],$$

and $U^{ij}_B = [\Delta v^i_{pcc,dq} \; \Delta i^{ij}_{IL,dq} \; \Delta v^j_{pcc,dq} \; \Delta i^{ji}_{IL,dq} \; \Delta\omega^i_{com} \; \Delta\omega^j_{com}]$, $Y^{ij}_B = \begin{bmatrix} \Delta v^i_{fc,dq} & \Delta v^j_{fc,dq} & \Delta v^j_{dc} & \Delta\delta^i_B & \Delta\delta^j_B \end{bmatrix}$ and the matrices can be calculated analytically using *sysic* function.

D. NMG Interconnection via BTBCs

The NMG model can be comprehensively represented in a homogeneous form as:

$$\dot{X}_{NMG} = A_{NMG}X_{NMG} \quad (18)$$

where X_{NMG} can be expressed as

$$X_{NMG} = [\overbrace{X^1_{MG} \; ... \; X^n_{MG}}^{MGs} \; \overbrace{... \; X^{ij}_{IL} \; ...}^{\text{ILs}} \; \overbrace{... \; X^{ij}_B \; ...}^{BTBCs}]^T.$$

It includes $(13m+2)n+2p+21q$ state variables, where n, p and q are the number of MGs, ILs and BTBCs respectively. A_{NMG} can be calculated easily for interconnecting the desired number of components using *sysic* function.

III. Simulation Results

In this section, two NMGs through one BTBC are simulated in MATLAB software. The structure of all MGs is as shown in Fig. 2. Electrical and control parameter values of the simulated systems are presented in [35].

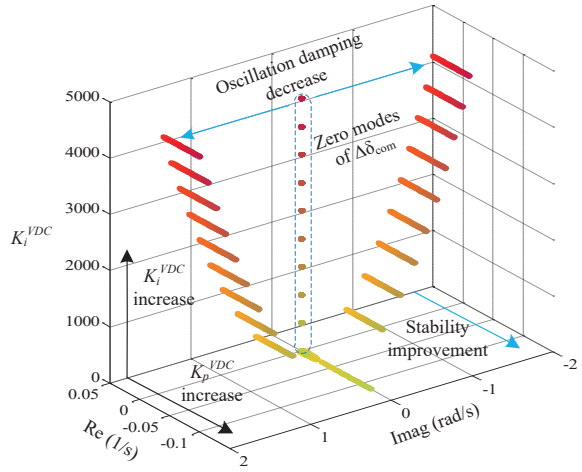

Fig. 4. Sensitivity analysis output for the BTBC voltage controller parameters: $0.1 < K_p^{DVC} < 200$, $1 < K_i^{DVC} < 4000$, and $R_{Ldc} = 0$.

TABLE I. PARTICIPATION MATRIX FOR BTBC DC SIDE AND CONTROLLER

State variable	Dynamic modes		
	$\lambda_{23} = -16667$	$\lambda_{70} = j1.05$	$\lambda_{71} = -j1.05$
ΔX_{dc1}	0.5	0.249	0.249
Δ_{dc2}	0.5	0.249	0.249
$\Delta\zeta$	0	0.499	0.499
Other	0	<0.003	<0.003

A. Sensitivity Analysis

1) BTBC DC side and voltage controller: Table I shows the participation factors for this case. The non-dominant frequency mode is only impacted by the DC power parameters. However, the dominant LFMs are related to both power and control parts of the DC link as well as the current controller. Fig. 4 indicates the trajectory of $\lambda_{70,71}$ for changing the DC voltage controller parameters as $0.1 < K_p^{DVC} < 200$ and $1 < K_i^{DVC} < 4000$. As a general result, the K_p^{DVC} increase results in the low stability improvement and K_i^{DVC} increase leads to reduce the oscillation damping. In order to maintain stability, the K_p^{DVC} must be chosen larger in relation to a larger K_i^{DVC}.

2) BTBC PLLs: Fig. 5 shows the loci of BTBC PLL affected eigenvalues for changing parameters as $0.01 < K_p^{PLL} < 1$ and $0.1 < K_i^{PLL} < 5$. In accordance with two

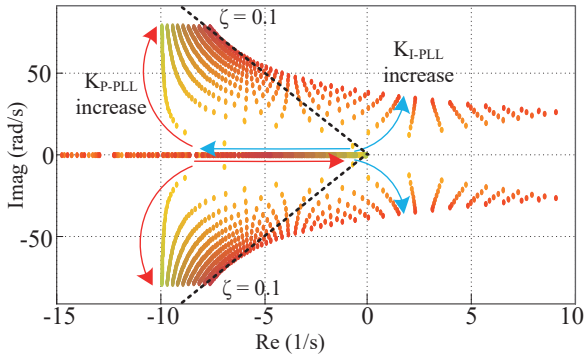

Fig. 5. Sensitivity analysis output for the BTBC PLL parameters: $0.01 < K_p^{PLL} < 1$ and $0.1 < K_i^{PLL} < 5$.

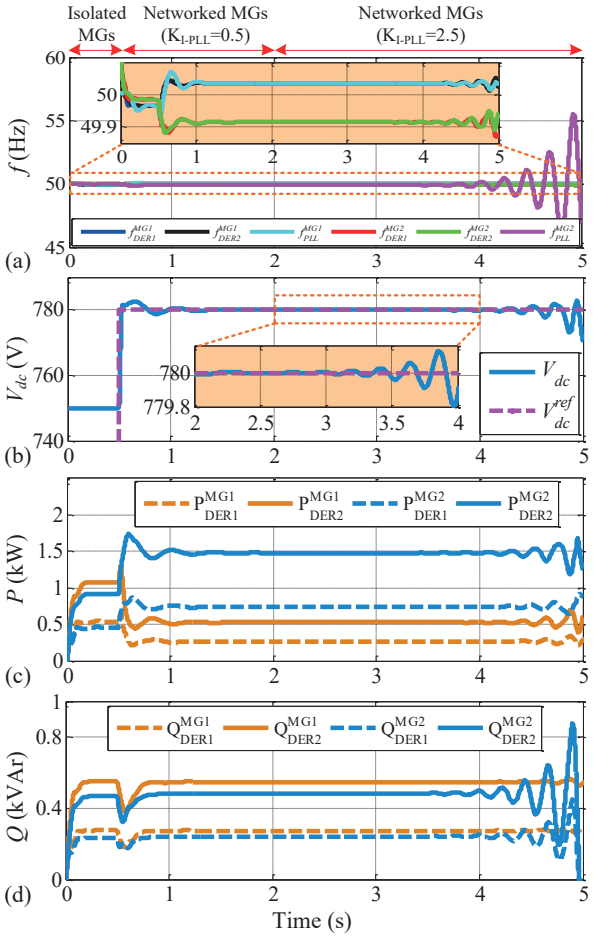

Fig. 6. Two Networked MGs: (a) DER and PLL frequencies, (b) DC voltage of BTBC, (c) active powers of DERs, (d) reactive powers of DERs.

oscillatory modes one can conclude: 1) the K_p^{PLL} increase leads to improve the stability boundary, although decrease the oscillation damping for all values of K_i^{PLL}. 2) Very low values of K_p^{PLL} cause instability, which their amounts increase by increasing the K_i^{PLL}. This means that the difference between K_p^{PLL} and K_i^{PLL} values do not be very large. 3) The K_i^{PLL} increment causes instability for a low range of K_p^{PLL}. In accordance with the non-oscillatory mode, the stability improves by decreasing K_p^{PLL} and/or increasing K_i^{PLL}. This mode stays stable even for large values of PLL parameters. Therefore, an acceptable range of the PLL parameters can be found as $0.2 < K_p^{PLL} < 0.7$ and $0.5 < K_i^{PLL} < 2$ in order to satisfy a degree of robust stability and as well as a specified value of oscillation damping ($\zeta = 0.1$ [36]).

B. Time Domain Simulations

Fig. 6 illustrates a number of results for the two NMGs, where the MGs are isolated until $t = 0.5$ s. Both of them are connected at $t = 0.5$ s with $K_i^{PLL2} = 0.5$ to exchange 800 W from MG_2 to MG_1, which results in a stable two NMG operation. The K_i^{PLL2} is increased to 2.5 at $t = 2$ s. According to Fig. 6(a), DER and PLL frequencies indicates

a slow instability due to exciting correlated LFMs to the $BTBC_{12}$ PLL shown in Fig. 5. Although instability is larger in f_{PLL}^{MG2} due to changing the related parameter, it can be shown in other frequency waveforms with a lower peak. The impact of frequency instability on the DC link voltage can be seen in Fig. 6(b), which it , in turn, spreads the instability to MG_1. Fig. 6(c) and (d) show MG_2 support for MG_1 until $t = 2$ s, then the instability.

IV. Conclusion

The smal-signal stability of MGs networked through BTBCs has been investigated in this paper. A detailed, comprehensive, and generalizable small-signal model is developed using *sysic* function of Robust Control Toolbox/MATLAB. BTBC-NMGs are identified based on dynamic modes, specially the LFMs using eigenvalue analysis and participation matrix. In addition to previous studies stating droop gains as the most effective parameters on the LFMs, the BTBC parameters are introduced as the important participants in the LFMs. The DC voltage controller and synchronizing PLL parameters have remarkable impact on the NMG stability and can unstable the NMGs for certain reported values.

References

[1] H. Bevrani, B. François, and T. Ise, *Microgrid dynamics and control*. John Wiley & Sons, 2017.

[2] R. Majumder, "Some aspects of stability in microgrids," *IEEE Trans. Power Syst.*, vol. 28, no. 3, pp. 3243–3252, 2013.

[3] M. Shahidehpour, Z. Li, S. Bahramirad, Z. Li, and W. Tian, "Networked microgrids: Exploring the possibilities of the iit-bronzeville grid," *IEEE Power and Energy Mag.*, vol. 15, no. 4, pp. 63–71, 2017.

[4] Y. Y. Hong, M. C. Hsiao, Y. R. Chang, Y. D. Lee, and H. C. Huang, "Multiscenario underfrequency load shedding in a microgrid consisting of intermittent renewables," *IEEE Trans. Power Del.*, vol. 28, no. 3, pp. 1610–1617, 2013.

[5] E. Bullich-Massagué, F. Díaz-González, M. Aragüés-Peñalba, F. Girbau-Llistuella, P. Olivella-Rosell, and A. Sumper, "Microgrid clustering architectures," *Applied Energy*, vol. 212, pp. 340–361, 2018.

[6] Q. Shafiee, T. Dragičević, J. C. Vasquez, and J. M. Guerrero, "Hierarchical control for multiple dc-microgrids clusters," *IEEE Trans. Energy Conv.*, vol. 29, no. 4, pp. 922–933, 2014.

[7] S. Moayedi and A. Davoudi, "Distributed tertiary control of dc microgrid clusters," *IEEE Trans. Power Electron.*, vol. 31, no. 2, pp. 1717–1733, 2016.

[8] E. Pashajavid, A. Ghosh, and F. Zare, "A multimode supervisory control scheme for coupling remote droop-regulated microgrids," *IEEE Trans. Smart Grid*, vol. 9, no. 5, pp. 5381–5392, 2018.

[9] M. J. Hossain, M. A. Mahmud, F. Milano, S. Bacha, and A. Hably, "Design of robust distributed control for interconnected microgrids," *IEEE Trans. Smart Grid*, vol. 7, no. 6, pp. 2724–2735, 2016.

[10] I. P. Nikolakakos, H. H. Zeineldin, M. S. El-Moursi, and N. D. Hatziargyriou, "Stability evaluation of interconnected multi-inverter microgrids through critical clusters," *IEEE Trans. Power Syst.*, vol. 31, no. 4, pp. 3060–3072, 2016.

[11] R. Zamora and A. K. Srivastava, "Multi-layer architecture for voltage and frequency control in networked microgrids," *IEEE Trans. Smart Grid*, vol. 9, no. 3, pp. 2076–2085, 2018.

[12] J. Zhou, H. Zhang, Q. Sun, D. Ma, and B. Huang, "Event-based distributed active power sharing control for interconnected ac and dc microgrids," *IEEE Trans. Smart Grid*, vol. 5, no. 6, pp. 6815–6828, 2018.

[13] P. C. Loh, D. Li, Y. K. Chai, and F. Blaabjerg, "Autonomous operation of hybrid microgrid with ac and dc subgrids," *IEEE Trans. Power Electron.*, vol. 28, no. 5, pp. 2214–2223, 2013.

[14] P. Wu, W. Huang, N. Tai, and S. Liang, "A novel design of architecture and control for multiple microgrids with hybrid ac/dc connection," *Applied Energy*, vol. 210, pp. 1002–1016, 2018.

[15] X. Wu, Y. Xu, X. Wu, J. He, J. M. Guerrero, C.-C. Liu, K. P. Schneider, and D. T. Ton, "A two-layer distributed control method for islanded networked microgrid systems," *Submitted to IEEE Trans. Smart Grid*, 2018.

[16] Z. Zhao, P. Yang, Y. Wang, Z. Xu, and J. M. Guerrero, "Dynamic characteristics analysis and stabilization of pv-based multiple microgrid clusters," *IEEE Trans. Smart Grid*, to be published.

[17] F. Shahnia and A. Arefi, "Eigenanalysis-based small signal stability of the system of coupled sustainable microgrids," *Int. J. Electr. Power & Energy Syst.*, vol. 91, pp. 42–60, 2017.

[18] H.-J. Yoo, T.-T. Nguyen, and H.-M. Kim, "Multi-frequency control in a stand-alone multi-microgrid system using a back-to-back converter," *Energies*, vol. 10, no. 6, p. 822, 2017.

[19] I. U. Nutkani, P. C. Loh, P. Wang, T. K. Jet, and F. Blaabjerg, "Intertied ac–ac microgrids with autonomous power import and export," *Int. J. Electr. Power & Energy Syst.*, vol. 65, pp. 385–393, 2015.

[20] J. Suh, D.-H. Yoon, Y.-S. Cho, and G. Jang, "Flexible frequency operation strategy of power system with high renewable penetration," *IEEE Trans. Sustainable Energy*, vol. 8, no. 1, pp. 192–199, 2017.

[21] I. U. Nutkani, P. C. Loh, and F. Blaabjerg, "Distributed operation of interlinked ac microgrids with dynamic active and reactive power tuning," *IEEE Trans. Industry Appl.*, vol. 49, no. 5, pp. 2188–2196, 2013.

[22] C.-Y. Tang, Y.-F. Chen, Y.-M. Chen, and Y.-R. Chang, "Dc-link voltage control strategy for three-phase back-to-back active power conditioners," *IEEE Trans. Ind. Electron.*, vol. 62, no. 10, pp. 6306–6316, 2015.

[23] R. Majumder and G. Bag, "Parallel operation of converter interfaced multiple microgrids," *Int. J. Electr. Power & Energy Syst.*, vol. 55, pp. 486–496, 2014.

[24] R. Majumder, "A hybrid microgrid with dc connection at back to back converters," *IEEE Trans. Smart Grid*, vol. 5, no. 1, pp. 251–259, 2014.

[25] N. Pogaku, M. Prodanovic, and T. C. Green, "Modeling, analysis and testing of autonomous operation of an inverter-based microgrid," *IEEE Trans. Power Electron.*, vol. 22, no. 2, pp. 613–625, 2007.

[26] M. Naderi, Y. Khayat, Q. Shafiee, and H. Bevrani, "Modeling of voltage source converters in microgrids using equivalent thevenin circuit," in *9'th Ann. Power Electron., Drives Syst. and Technol. Conf. (PEDSTC)*. IEEE, 2018, pp. 510–515.

[27] M. Naderi, Y. Khayat, Q. Shafiee, H. Bevrani, and F. Blaabjerg, "Modeling of islanded microgrids using static and dynamic equivalent thevenin circuits," in *20'th Euro. Conf. Power Electron. and Appl. (EPE'18 ECCE Europe)*. IEEE, 2018, pp. 1–10.

[28] Y. Khayat, M. Naderi, Q. Shafiee, Y. Batmani, M. Fathi, J. M. Guerrero, and H. Bevrani, "Decentralized optimal frequency control in autonomous microgrids," *IEEE Trans. Power Syst.*, 2018.

[29] M. Naderi, Y. Khayat, Q. Shafiee, T. Dragicevic, H. Bevrani, and F. Blaabjerg, "Small-signal modeling and prony analysis-based validation of interconnected microgrids," *Submitted to IEEE Trans. Power Syst.*, 2019.

[30] M. S. Golsorkhi, D. J. Hill, and H. R. Karshenas, "Distributed voltage control and power management of networked microgrids," *IEEE J. Emerging and Sel. Topics in Power Electron.*, vol. 6, no. 4, pp. 1892–1902, 2018.

[31] Y. Zhang, L. Xie, and Q. Ding, "Interactive control of coupled microgrids for guaranteed system-wide small signal stability," *IEEE Trans. Smart Grid*, vol. 7, no. 2, pp. 1088–1096, 2016.

[32] T. Dragičević, "Model predictive control of power converters for robust and fast operation of ac microgrids," *IEEE Trans. Power Electron.*, vol. 33, no. 7, pp. 6304–6317, 2017.

[33] M. Naderi, Y. Khayat, Q. Shafiee, T. Dragicevic, H. Bevrani, and F. Blaabjerg, "Interconnected autonomous ac microgrids via back-to-back converters—part I: small-signal modeling," *IEEE Trans. Power Electron.*, 2019, DOI: 10.1109/TPEL.2019.2943996.

[34] F. Shahnia, "Stability and eigenanalysis of a sustainable remote area microgrid with a transforming structure," *Sustainable Energy, Grids and Netw.*, vol. 8, pp. 37–50, 2016.

[35] M. Naderi, Y. Khayat, Q. Shafiee, T. Dragicevic, H. Bevrani, and F. Blaabjerg, "An emergency active and reactive power exchange solution for networked microgrids," *Submitted to IEEE j. emerging and sel. topics in power electron.*, 2019.

[36] B. Pal and B. Chaudhuri, *Robust control in power systems*. Springer Science & Business Media, 2006.